Watching Paint Dry

Reichenberger, Markus; Baderschneider, Sebastian; Kroh, Daniel; Grauf, Steffen; Koehler, Juergen; Hildner, Richard; Koehler, Anna

Published in:
Macromolecules

DOI:
10.1021/acs.macromol.6b01257

Publication date:
2016

Macromolecules

Article

pubs.acs.org/Macromolecules

Watching Paint Dry: The Impact of Diiodooctane on the Kinetics of Aggregate Formation in Thin Films of Poly(3-hexylthiophene)

Markus Reichenberger,[†] Sebastian Baderschneider,[‡] Daniel Kroh,[†] Steffen Grauf,[†] Jürgen Köhler,[‡,§] Richard Hildner,[‡] and Anna Köhler*[,†,§]

[†]Experimental Physics II, University of Bayreuth, 95440 Bayreuth, Germany

[‡]Experimental Physics IV, University of Bayreuth, 95440 Bayreuth, Germany

[§]Bayreuth Institute of Macromolecular Research (BIMF), University of Bayreuth, 95440 Bayreuth, Germany

Supporting Information

ABSTRACT: We have investigated how the addition of 1,8-diiodooctane (DIO) alters the formation of disordered and ordered phases in a film of poly(3-hexylthiophene-2,5-diyl) (P3HT). By combining in situ time-resolved absorption spectroscopy with 60 ms time resolution, optical and transmission electron microscopy and spatially resolved photoluminescence spectroscopy, we show that, in addition to the excitonic coupling, the film formation process during spin-coating as well as the subsequent long-time film drying process differ significantly when DIO is added to a solution of P3HT. During spin-coating, the addition of DIO reduces the actual time for transformation from disordered to ordered phase, even though it increases the time until the disorder−order transition sets in. In place of a solidification front, we observe an all-over solidification throughout the entire film. The phase separation between nonaggregated and aggregated phase increases when using DIO, with compositional variation in the content of aggregated phase on a micrometer scale.

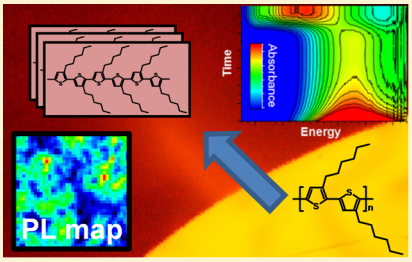

INTRODUCTION

The mesoscopic order and crystallinity in films of semiconducting polymers is well-known to have a strong impact on the resulting electronic structure and thus on the performance of devices such as organic solar cells (OSCs) and of organic field effect transistors (OFETs). In particular, the formation of well-ordered aggregates increases the efficiency of electron−hole dissociation,[1−12] a key process in OSCs, and the mobility of charges, which controls OFET performance.[13−18] Many semiconducting polymers form semicrystalline films that contain domains of ordered, aggregated chains embedded in a matrix of disordered chains.[4,7,19−24] A way to increase the fraction of aggregated chains in a spin-coated film is to add a small amount of higher boiling point solvents such as 1,8-diiodooctane (DIO) to a polymer solution.[25] Peet and co-workers pioneered this approach, for example to increase the amount of ß-phase in polyfluorene.[26] Today, solvent additives such as s 1,8-diiodooctane (DIO), 1,8-octanedithiol (ODT) and 1,8-dichlorooctane (DCO) are most frequently used for the fabrication of donor−acceptor type blends hat are conducive to high solar cell efficiencies,[4,5,25,27−32] and there is a wealth of studies about the impact of a solvent additive on a *blend* film.[3,5,25,33] For example, it has been shown that films cast from a solution containing a solvent additive possess phases with a higher structural order.[34] The overall film morphology can be highly complex, containing a number of different phases.[25,35] Often, self-assembly leads to optimized charge percolation paths in the active layer of organic solar cells.[36] In the process of film formation, the crystallization of poly(3-hexylthiophene) (P3HT) expels PCBM into the nonaggregated regions of the interlayers, whereas the P3HT crystallinity is not strongly affected by the PCBM.[37,38] Even though this crystallization process in P3HT has been identified a key parameter, studies that explicitly focus on the mechanism by which P3HT aggregates form during spin coating and what the role of the high boiling point additives is in these processes have been reported only recently. In general, it is considered that solvent additives, such as 1,8-diiodooctane (DIO), 1,8-octanedithiol (ODT), and 1,8-dichlorooctane (DCO), reduce the drying rate of a polymer solution so that the polymer chains have more time for self-organization.[26,39]

In classical polymer science, it is well-known that aggregate formation in thin films depends not only on the thermodynamic parameters but also on the kinetics of film formation,[40−42] and this also applies to aggregate formation in semiconducting polymers.[7,26,30] For example, for the polyfluorene PFO, solvents with the same solubility parameters, yet a higher boiling point, lead to a higher fraction of ß-phase upon spin-coating.[7] This was accounted for by increased time for a nucleation and growth process when the boiling point is higher and is consistent with the suggestion of an increased drying time proposed by Peet et al.[30]

Received: June 13, 2016
Revised: August 12, 2016
Published: August 23, 2016

DOI: 10.1021/acs.macromol.6b01257
Macromolecules 2016, 49, 6420−6430

In contrast to PFO, for P3HT on its own, the use of DIO is considered to have little effect as the resulting fraction of aggregates is similar when DIO is used as when it is omitted.[30] Here, we combine time-resolved in situ absorption spectroscopy, spatially resolved photoluminescence spectroscopy, and optical microscopy to elucidate the process of film formation both on a short time scale with 60 ms resolution and on a long time scale up to 48 h. We demonstrate that even though the final amount of aggregates in the P3HT film is about the same with and without DIO, the phase separation between aggregated and nonaggregate chains and the exciton coupling within the crystallites differs significantly due to the difference in the film formation process.

EXPERIMENTAL METHODS

Materials. The solutions and films were made of poly(3-hexylthiophene-2,5-diyl) (P3HT) purchased from Rieke Metals of average molecular weight (M_n) of 18 800 g/mol with a polydispersity index (PDI) of 2.04, a 4002-EE grade and a regioregularity of more than 98% in a head-to-tail connection. The solvent is chlorobenzene (CB, boiling point of 132 °C at 1 atm) and the solvent-additive is 1,8-diiodooctane (DIO, boiling point of about 364 °C at 1 atm), both purchased from Sigma-Aldrich. Figure 1 shows the chemical structure

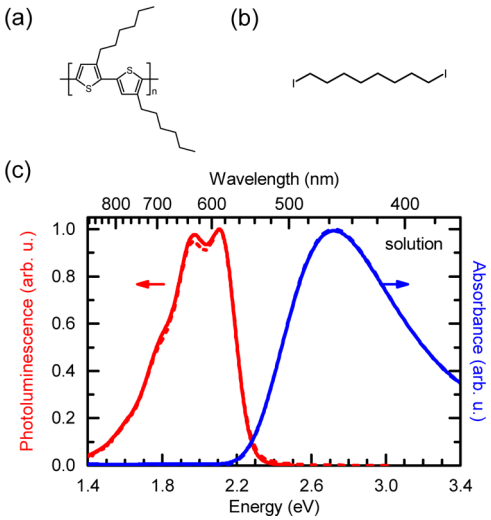

Figure 1. Chemical structure of (a) regioregular poly(3-hexylthiophene-2,5-diyl) (P3HT), and (b) 1,8-diiodooctane (DIO). (c) Photoluminescence for excitation at 3.06 eV (red lines) and absorption (blue lines) spectra of P3HT taken in chlorobenzene solution without (dashed lines) and with 3 vol % (solid lines) DIO. The spectra are normalized to unity at their maximum.

of regioregular P3HT and DIO. For the solar cell devices molybdenum(VI) oxide (MoO_3) and bathocuproine (BCP) were bought from Sigma-Aldrich and C_{60} from American Dye Source.

Sample Preparation. The samples were prepared in a glovebox by first preparing the solutions made of P3HT and chlorobenzene, filtered with a filter of 0.2 μm pore size, with or without three to five percent by volume of 1,8-diiodooctane (DIO) as solvent additive. For the solution measurements a concentration of 0.33 g/L (approximately 8×10^{-6} M) was chosen and 10 g/L (about 2×10^{-4} M) for film measurements. The solutions were stirred at 40 °C and about 400 rpm for several hours and filtered through a 0.2 μm filter afterward. The solutions were filled into a 1 mm quartz cuvette or deposited onto a round quartz substrate, with a diameter of 1.3 cm, by spin-coating to obtain P3HT films with a thickness of about 80 nm. These thin films were resting for 10 min to allow for some rearrangements of the polymer chains and to make sure that the film contains only very little solvent during measurements as monitored by measuring the signature of DIO absorption near 4 eV.

Optical Spectroscopy. Ultraviolet−visible (UV−vis) absorption spectra were acquired using a Cary 5000 UV−vis spectrometer from Varian. Absorption spectra taken during spin-coating in air were obtained using a home-built setup. It consist of a white light LED as light source inside a spin-coater and a detection unit (a fiber-coupled MS125 sepctrograph from Oriel Instruments and a charge-coupled device (CCD) camera from Andor-Solis in kinetic mode) that takes one picture every 60 ms. For emission, the samples were excited with a continuous-wave diode laser from Coherent at 405 nm (3.06 eV) and the steady-state photoluminescence spectra were taken by the same spectrograph and CCD camera as for absorption. During the emission measurements, each sample was held under nitrogen.

Morphological Characterization. Pictures of the polymer film surface were acquired using an optical microscope from ZEISS with an EOS 5D single lens reflex camera from Canon on top. The light source was a 150 W xenon lamp. For the image acquisition we used the incident light technique with an 80x objective and, for better image contrast, with a silicon waver below the substrate. Layer thicknesses were measured with a Dektak 150 profilometer from Veeco. Atomic force microscopy (AFM) was done with a Dimension Icon AFM and Scan Asyst from Bruker in tapping mode (because of soft polymer films). We used the software NanoScope Analysis from Bruker to flatten the AFM pictures and to determine the surface roughness R_a, the arithmetic average of the absolute values of the surface height deviations Z, measured over the average area: $R_a = \frac{1}{N}\sum_{j=1}^{N}|Z_j|$

Transmission electron microscopy (TEM) imaging was carried out with a LEO Zeiss EM 922 Omega. Films were spun out of a P3HT-CB solution with 5 vol % DIO onto carbon grids, which were lying on a glass substrate. After spin-coating, the sample was dried on a hot plate at 45 °C for 5 min.

Spatially Resolved Photoluminescence Measurements. Spatially resolved photoluminescence spectra were taken using a home-built confocal microscope setup[43] with a pulsed laser diode from PicoQuant (450 nm, 2.75 eV), a spectrograph Acton SP2150 from Princeton Instruments, and a CCD camera Sensicam QE of PCO. The spatial resolution is about 600 nm. For the measurements, the samples were held under nitrogen. We measured the spatially resolved photoluminescence maps by scanning the film in the two dimensions parallel to the film surface via deflecting the laser beam with a scan mirror in combination with a pair of telecentric lenses. Neighboring measurement spots had a distance of 1 μm to each other, so that one measurement with a laser spot diameter of 600 nm did not affect another measurement. Each pixel of a spatially resolved photoluminescence map belongs to a specific photoluminescence spectrum. Similar emission spectra are shown in the same color. The emission spectra are distinguished by the integrated intensity of their high-energy peak region at about 2.15 eV. A colored scale bar for this integrated intensity corresponds to the relative intensity of the nonaggregated chains, with minimum and maximum integrated photoluminescence intensity of nonaggregated chains at its ends and continuously varying integrated intensity in between. The 25 spectra that define the scale bar and that are classified by a home-built pattern recognition algorithm are shown in Figure S1 in the Supporting Information. For this experiment we added 5 vol % DIO to the casting solvent since this gives a better contrast in the spatially resolved photoluminescence maps of the spun films without significantly changing the optical and electrical properties of the film.

Solar Cell Preparation and Measurements. The solar cells were prepared in a bilayer system as described by Schwarz et al.[44] The base is a glass substrate covered with indium tin oxide (ITO). A 15 nm thick MoO_3 layer was brought up onto the ITO layer by vacuum evaporation, to lower the dark current and to improve the diode behavior of the solar cell. The P3HT layer was spun from CB solution with or without DIO, as described in the sample preparation. After this step, the devices were resting 30 min, followed by annealing for 5 min at 60 °C. The thickness of this P3HT layer is 46 nm if spun without DIO and 52 nm if spun with DIO. Finally, a 30 nm thick C_{60} layer as

DOI: 10.1021/acs.macromol.6b01257
Macromolecules 2016, 49, 6420−6430

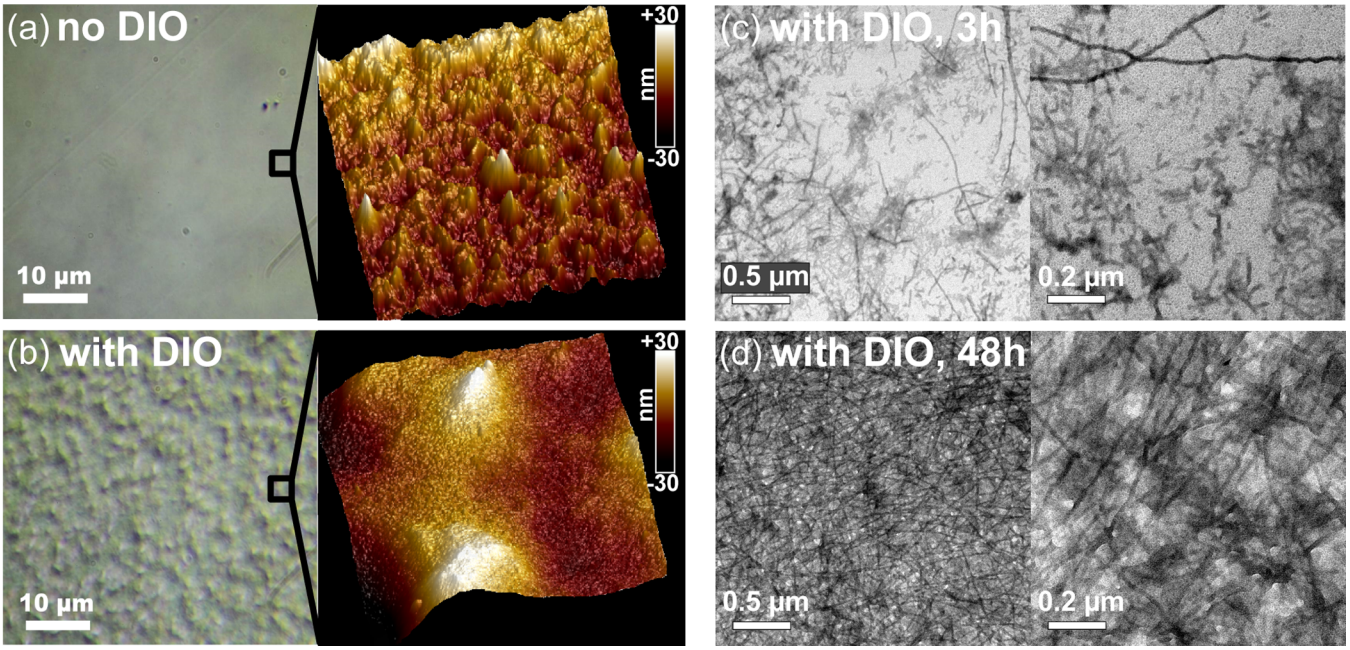

Figure 2. Optical microscope surface images (see scale bar for size) and atomic force microscope surface height images (3 μm × 3 μm area, indicated by the black square in the optical microscope image) of a P3HT film spin-cast from a chlorobenzene solution (a) without and (b) with 3 vol % DIO. TEM images of a film with 5 vol % DIO (c) taken 3 h after preparation and (d) taken 48 h after preparation.

acceptor, a 5 nm thick BCP layer and a 100 nm thick aluminum cathode were vacuum evaporated. The whole fabrication was carried out in a nitrogen atmosphere using a glovebox with an integrated evaporation chamber. For the measurements the solar cells were placed in an evacuated sample holder. We took the current−voltage characteristics under AM1.5 sunlight conditions in a Newport sun simulator with a Keithley 238 source-measure-unit. Before the second measurement, the solar cells were resting 18 h in the glovebox, on a hot plate at moderate 60 °C to accelerate C_{60} diffusion into the film.

RESULTS

To study the influence of DIO on the optical spectra of P3HT in solution and film, we measured UV−vis absorption and photoluminescence in both, solutions and spin-cast films. For this, we used chlorobenzene (CB), in each case once without and with three percent by volume of DIO at room temperature. For reference, Figure 1 shows the absorption and emission spectra obtained in solution. The addition of 3 vol % DIO to the CB does not lead to any changes in the spectra. With and without DIO, we observe the broad unstructured absorption spectrum centered at 2.7 eV (540 nm) and the weakly structured emission spectra with the 0−0 peak at 2.1 eV (590 nm) that are characteristic for disordered, nonaggregated chains of P3HT.[23,45]

In contrast to solution, films spun from CB with or without DIO show marked differences (Figure 2). A P3HT film spun from CB without DIO appears homogeneous when observed through an optical microscope, while structure on a 1 μm scale is visible when the film is spun from CB with DIO. This is also displayed in a higher resolution by the AFM height images, where the difference between the coarse, large-scale surface topology evident in the film spun with DIO contrasts markedly with the finer structure displayed in the film spun without DIO. The AFM height imaging further yields that the average surface roughness increases from 3.9 nm in a P3HT film spun without DIO to 7.4 nm in a P3HT film spun with DIO. TEM images from P3HT films spun with DIO were taken 3 h after film preparation as well as 48 h after film preparation. After 3 h, we observe a low density of fibrillary structures that transforms into a dense network eventually.

The difference between the films spun with and without DIO is also reflected in the electronic structure of the P3HT, as evident from absorption and photoluminescence spectra (Figure 3). Compared to the solutions, films of P3HT spun from CB solution with or without DIO both show red-shifted absorption and photoluminescence spectra (Figure 3a,b), indicating that the film spectra are dominated by aggregated chains. Both film absorption spectra show the well-known vibronic structure of weakly interacting H-type aggregates in P3HT with peaks at 2.06 eV (602 nm), 2.24 eV (554 nm), and 2.40 eV (517 nm).[23,45,46] However, in the film spun from the solution with DIO, the absorption peak at 2.06 eV and the high-energy tail increase in intensity compared to the film spun from solution without DIO (Figure 3d,f).

The absorption spectra can be decomposed into the contributions from aggregated chains and from nonaggregated chains as detailed in refs 23 and 45 For this, we scale the absorption obtained in solution to the high energy tail of the thin film spectrum shown in parts d and f of Figure 3 and subtract it (see Figure S2 in the Supporting Information). The resulting difference spectrum is attributed to absorption from the aggregated chains. Analyzing the aggregate absorption spectrum in terms of a Franck−Condon progression yields the intensities A_1 and A_2 of the two lowest energy peaks in the P3HT absorption band. From this, the exciton bandwidth W can be derived using

$$\frac{A_1}{A_2} = \frac{n_{0-0}}{n_{0-1}} \frac{\left(1 - \frac{W}{2\omega_0} e^{-S} \sum_{\nu>0} \frac{S^\nu}{\nu!\nu}\right)^2}{S\left(1 - \frac{W}{2\omega_0} e^{-S} \sum_{\nu(\neq 1)} \frac{S^\nu}{\nu!(\nu-1)}\right)^2}$$

as described in refs 23 and 45.

DOI: 10.1021/acs.macromol.6b01257
Macromolecules 2016, 49, 6420−6430

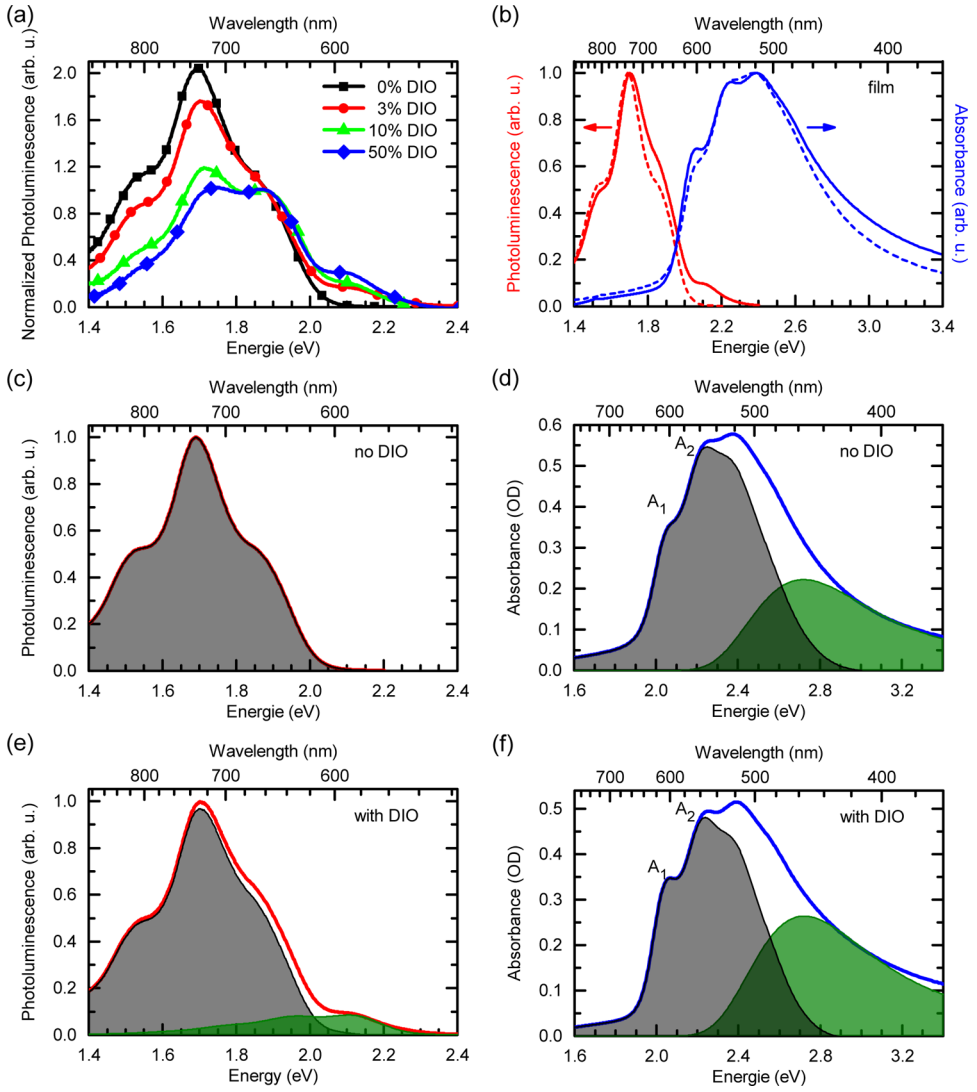

Figure 3. (a) Photoluminescence spectra of P3HT films spin-cast out of chlorobenzene solutions with different volume percent of DIO: 0 vol % (black line with squares), 3 vol % (red line with circles), 10 vol % DIO (green line with triangles) and 50 vol % DIO (blue line with diamonds). The spectra are normalized to the shoulder at 1.9 eV. (b) Photoluminescence for excitation at 3.06 eV (red lines) and absorption (blue lines) spectra of P3HT taken from a thin film spun from chlorobenzene solution without (dashed lines) and with 3 vol % (solid lines) DIO. The spectra are normalized to unity at their maximum. (c, e) Photoluminescence (red line) and (d, f) absorption spectra (blue line) of a P3HT film spun from a CB solution (c, d) without and (e, f) with 3 vol % DIO. The spectra are decomposed into contributions attributed to nonaggregated polymer chains (green filled line) and aggregated polymer chains (black filled line). The first two absorption peaks are labeled as A_1 and A_2. Note that part c does not show photoluminescence from nonaggregated chains of the P3HT film.

The resulting value for the free exciton bandwidth W is 124 meV for a P3HT film without DIO and 56 meV for a P3HT film with DIO. This translates into an excitonic coupling strength J, given by $W = 4J\cos\left(\frac{\pi}{N+1}\right) \overset{N\to\infty}{\approx} 4J$ of 31 meV for the film spun without DIO and 14 meV for the film spun with DIO. According to refs 47 and 48, the decreased exciton bandwidth and coupling strength correspond to an increase in conjugation length from 22 repeat units in the film spun without DIO to 40 repeat units in the film spun with DIO. These values are summarized in Table 1 for ease of reference. The *fraction of absorption* from the aggregated chains reduces from 65% in the film spun without DIO to 56% in the film spun with DIO and measured immediately after film preparation. If we consider that the oscillator strength of aggregated chains is typically about 1.4 times the oscillator strength of the nonaggregated chains,[23] this implies that the *fraction of aggregated chains* reduces from 46% to 40%. Thus, when P3HT is spun from CB containing 3 vol % DIO, the resulting films initially contain a *lower* fraction of aggregated chains that

Table 1. Optical and Electrical Properties of a P3HT Film Spun from a Chlorobenzene Solution without and with 3 vol % DIO

property of a P3HT film	without DIO	with DIO
absorption of aggregated chains	65%	56%
fraction of aggregated chains	46%	40%
ratio of peaks A_1/A_2	0.65	0.73
gaussian line width	75 meV	75 meV
effective oscillating mode $\hbar\omega_0$	175 meV	175 meV
Huang–Rhys parameter S	1.27	1.27
excitonic coupling strength J	31 meV	14 meV
conjugation length of aggregated chains	22	40

DOI: 10.1021/acs.macromol.6b01257
Macromolecules 2016, 49, 6420–6430

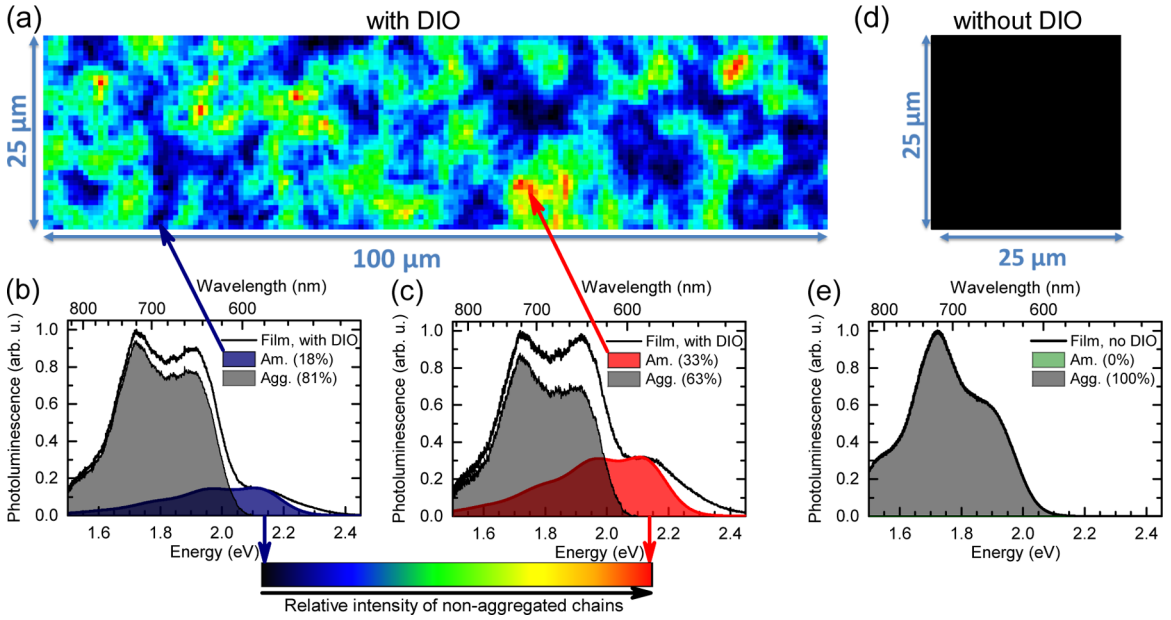

Figure 4. Spatially resolved photoluminescence maps of a P3HT film spun from chlorobenzene solution (a) with and (d) without 5 vol % DIO. The dimensions are shown in each picture. The color of the scale bar on the bottom of this picture corresponds to the relative intensity of the nonaggregated chains, whereby red indicates the highest and black the lowest integrated intensity of the nonaggregated chains. Normalized emission spectra with the lowest (b) and highest (c) integrated intensity of the nonaggregated chains obtained for a P3HT film spun from CB solution with DIO. The spectra are decomposed into the contributions by the nonaggregated chains (colored filled line) and the aggregated chains (gray filled line). (e) Emission spectrum of a pixel in part d. All pixels of the spatially resolved photoluminescence map show the same emission spectrum with zero intensity of nonaggregated chains, hence the uniform black appearance. Excitation was at 2.75 eV.

have, however, a longer conjugation length and concomitantly weaker excitonic coupling than the aggregates in a P3HT film spun from CB solution without DIO.

Additional information can be obtained from analyzing the photoluminescence spectra (Figure 3c,e). By comparison with published photoluminescence spectra, the spectrum obtained from the P3HT film spun without DIO can be attributed to emission from solely aggregated chains.[49,50] This implies that energy transfer from the 54% of photoexcited nonaggregated chains to the 46% of aggregated chain dominates over radiative decay on the nonaggregated chains in the film. This is the case when the scale of phase separation between the aggregated and nonaggregated chains is smaller than twice the exciton diffusion length, typically about 20 nm.[19] In contrast, when the films are spun from CB containing DIO, we observe a distinct additional peak in the PL spectrum at 2.1 eV (585 nm) that is a signature of emission from the nonaggregated chains in P3HT.[49] Such an emission can only occur if purely amorphous regions prevail that exceed the length scale for exciton diffusion to regions containing the lower energy aggregated chains. In an analogous way as for the absorption spectra, the contributions of nonaggregated and aggregated chains to the photoluminescence spectra can be separated out as detailed in the Supporting Information. In brief, the emission obtained from nonaggregated chains in solution (Figure 1) was normalized to reproduce the high energy tail of the film PL spectra and subtracted. The resulting difference spectra was associated with the aggregate emission. The correctness of the procedure was confirmed by comparing the resulting aggregate emission with a Franck−Condon analysis, taking into account that the 0−0 peak for H-aggregates is partially suppressed.[46] We note that the slight increase in 0−0 emission intensity of the aggregate emission of the P3HT film with DIO results from the smaller exciton bandwidth for this sample compared to the P3HT film without DIO. Hence, in the film with DIO, optically allowed states at the top of the exciton band are thermally populated with higher probability. When a higher content of DIO is used, e.g., 10−50 vol % in CB, the fraction of emission from nonaggregated chains increases accordingly, suggesting an even larger phase separation to occur (Figure 3a). Hence, a fine-tuning of the phase separation in a P3HT film is possible by controlling the volume percentage of DIO in the CB.

To obtain more information on the spatial distribution of the aggregated chains we took spatially resolved photoluminescence maps of a P3HT film. For this, a diode laser with 2.75 eV (450 nm) was coupled into a confocal microscope to excite an area of 600 nm diameter on the film. The resulting photoluminescence was collected by the microscope and recorded with a CCD camera. By scanning a certain film area and recording photoluminescence spectra every μm, a map can be generated. Figure 4a shows a map for a 25 μm × 100 μm section of the film spun from CB with 5 vol % DIO. Across the sample area, the spectra differ mainly regarding the relative intensity of the peak at 2.1 eV (Figure 4b,c), indicative of the emission from nonaggregated chains. Thus, we color-coded the map correspondingly with blue colored areas indicating that the spectra obtained from there contain little emission from the nonaggregated chains and red colored areas highlighting the regions with spectra that contain more intense emission from nonaggregated chains. Across the entire area scanned we did not observe any spot that was entirely without emission from nonaggregated chains, keeping in mind that our spatial resolution is in the range of 500 nm. When we applied the same approach to a 25 μm × 25 μm area of a film spun from CB without DIO, we obtain identical spectra all over that area, without any signature of luminescence from nonaggregated chains (Figure 4d,e), although at 2.75 eV, we excited mainly the amorphous P3HT. From Figure 4, we infer that in P3HT films

DOI: 10.1021/acs.macromol.6b01257
Macromolecules 2016, 49, 6420−6430

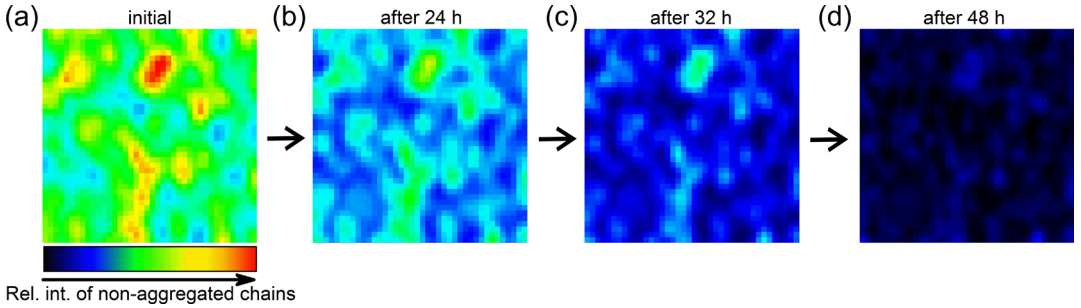

Figure 5. Spatially resolved photoluminescence map of a (25 μm × 25 μm) area of a P3HT film cast from a chlorobenzene solution with 5 vol % 1,8-diiodooctane (DIO), (a) initially, after (b) 24 h, (c) 32 h, and (d) 48 h from spin-coating. The color of the scale bar indicates the relative intensity of the nonaggregated chains. Excitation was at 2.75 eV.

spun from CB with 5 vol % DIO, there is an initial compositional variation in the content of nonaggregated chains in the order of several μm. This should not be confused with the scale of phase separation between nonaggregated and aggregated chains which is larger than twice the exciton diffusion length, typically 10−20 nm, (since we can observe the higher energy emission from the nonaggregated chains) yet smaller than our spatial resolution of 500 nm (as for each pixel we always observe both, emission from nonaggregated *and* from aggregated chains). In this way, we gain simultaneously information on the on the mesoscopic as well as on the nanoscopic length scale, in contrast to mere near-field absorption measurements.[51]

The data presented in Figure 4 were taken from freshly prepared films. To probe whether there is an evolution of the morphology on a longer time scale, a 25 μm × 25 μm area at different time intervals is displayed in Figure 5. The same absolute color code is used for all parts of Figure 5, and the associated spectra are shown in Figures S1 and S3 of the Supporting Information. It is clearly evident how the sample area "fades" into a blue color; i.e., the relative amount of emission from nonaggregated chains reduces gradually all over the film. It implies a continuous increase of weakly interacting H-aggregates that can be populated by energy transfer from any remaining photoexcited nonaggregated chains. The emission from the nonaggregated chains does not reduce uniformly over the film with time. Rather the emission reduces faster in areas that contain a higher fraction of nonaggregated chains (see Figure S3 in the Supporting Information)

The data shown in Figure 5 were taken in a N_2-filled sample chamber to avoid accidental photooxidation, and after 48 h, some small fraction of emission from disordered chains can still be observed (see Figure S3 in the Supporting Information). If the photoluminescence is taken in air, the emission from disordered chains has entirely disappeared after 48 h and the fraction of aggregated chains evident in the absorption spectra increases to 49% (see Figure S4a in the Supporting Information). We attribute this difference to the fact that DIO diffusion out of the film is easy in ambient air, while this is impeded in a closed, N_2 filled sample chamber.[52] It is important to note that the fraction of aggregated chains in a film spun from CB with DIO increases from initially 40% to 49% after a couple of days, whereas in the film spun from only CB, the fraction of aggregates obtained remains at 46% without change. Moreover, the aggregates thus formed using DIO have a longer conjugation length and lower excitonic coupling as evidenced by the higher ratio between the absorption peaks A_1/A_2 (see Figure S4b in the Supporting Information). These features would be consistent with a higher degree of order. The properties of the different films are summarized in Table 2.

Table 2. Optical Properties of a P3HT Film Spun from a Chlorobenzene Solution without and with 3 Vol% DIO, Directly after Spin-Coating and after 60 h/48 h in Air

	without DIO		with DIO	
property of a P3HT film	initial	after 60 h	initial	after 48 h
absorption of aggregated chains	65%	65%	56%	69%
fraction of aggregated chains	46%	46%	40%	49%
ratio of peaks A_1/A_2	0.65	0.65	0.73	0.77

To elucidate why the addition of DIO as cosolvent induces such a significant compositional variation upon spin-coating, we monitored the spin-coating process using *in situ* time-resolved absorption measurements. Figure 6a shows how the absorption evolves when a P3HT film is spun from CB-solution. We can distinguish three time regimes. For the first 25 s, we only observe the broad unstructured absorption centered at about 2.7 eV (460 nm) that indicates the presence of nonaggregated chains. The spectral shape of this absorption is constant throughout and the intensity is essentially unchanged, expect for an initial reduction due to cast-off of excess material and a hardly noticeable increase at 25 s, just before the second time regime starts. In the time range from 25 to 45 s, the intensity of the higher energy absorption band from the nonaggregated chains reduces while the structured lower energy band due to aggregate absorption increases. In this time regime, the spectra form an isosbestic point, indicative of a direct transformation from nonaggregated chains to weakly interacting H-aggregates. In the third time regime from 45 s until 60 s, i.e., the end of our observation time, no further changes occur to the spectra in intensity or shape. The evolution of the spectra in the three regimes is illustrated in Figure 6b. If the P3HT film is spun under the same conditions, yet from a CB solution containing 3 vol % DIO, the absorption evolves in an analogous manner, yet with modified time spans for the three regimes (Figure 6c,d). The initial period, during which merely absorption by nonaggregated chains is observed, extends much longer, up to 39 s. In contrast, the second period, during which the phase transition takes place, appears accelerated and takes only 16 s in total as compared to 20 s when DIO is absent. Again, there is no further noticeable evolution during the third period when the aggregate absorption is fully formed. Qualitatively the same changes, i.e. an increase of the initial period until the phase transition takes place followed by a faster actual transition, occur if the film is spun from a CB solution at lower

DOI: 10.1021/acs.macromol.6b01257
Macromolecules 2016, 49, 6420−6430

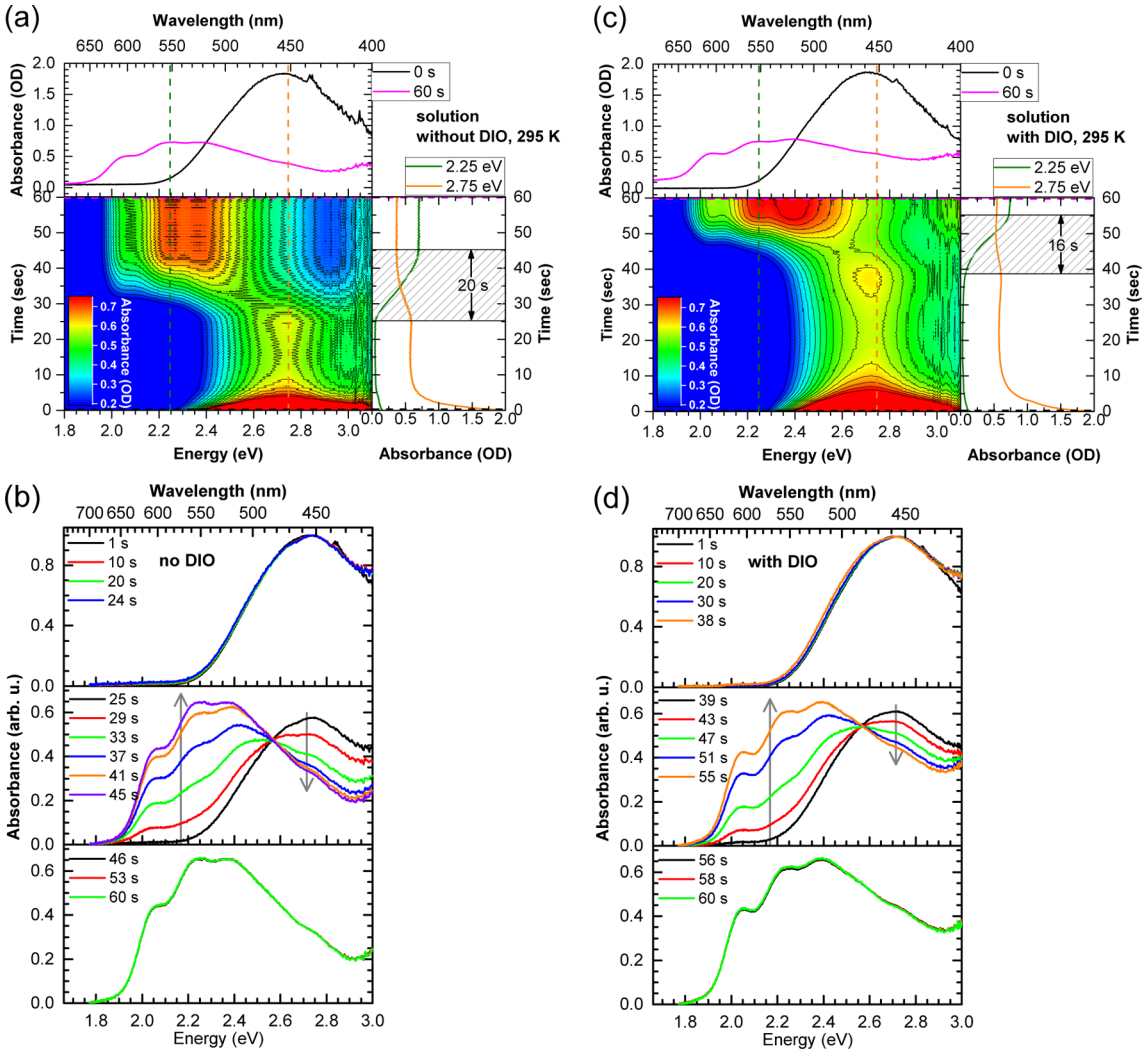

Figure 6. Absorption spectra of P3HT taken at different times during spin-coating from chlorobenzene solution (a) without and (c) with 3 vol % DIO at 295 K, displayed with time and energy as abscissae and ordinate, respectively, and with the optical density (OD) color coded from blue (OD $\leq$ 0.2) to red (OD $\geq$ 0.7). For reference, a wavelength scale is shown at the top. Horizontal and vertical cuts through the 3D-image, giving the spectra at a fixed time or the intensity decay at a fixed photon energy are shown on top and on the right. (b, d) Spectra shown in parts a and c are displayed grouped into three time ranges, as described in the text. The baseline of these spectra are set to zero at 1.8 eV to account for the offset due to scattering, and the spectra in the top panel are normalized to their maximum.

temperature such as 275 K or if the film is spun from a CB solution containing both P3HT and the C_{60} derivative PCBM in a 1:1 weight ratio (see Figure S5 in the Supporting Information).

The kinetics of film formation can also be monitored optically. Figure 7 shows a sequence of optical microscope pictures taken from the sample during the spin-coating process, with the quartz substrate being illuminated from below. Initially, the solution appears bright orange, which changes to a paler orange as soon as the excess solvent is thrown off by the rotation of the substrate. When the film solidifies, it changes color to purple due to the formation of aggregates that absorb in the red spectral range. If the film is spun from CB without DIO, a clear solidification front proceeds in a circular manner from the outside of the substrate to the inside until all CB is evaporated, leaving an apparently homogeneous film. In contrast, when the solution contained DIO, such a solidification front does not occur. Rather, the entire surface area darkens and changes continuously into a purple color. The resulting film is inhomogeneous.

To assess how the different film morphologies affect solar cell performance, we studied bilayer devices of P3HT and C_{60}. We used a bilayer geometry because this allows us to directly compare how C_{60} interacts with a P3HT films of different morphologies caused by adding DIO. Figure 8 shows the current−voltage characteristics at AM1.5 sunlight condition for P3HT/C_{60} bilayer solar cells, where the P3HT was spun from solution with and without DIO, prior to the evaporation of the C_{60}. Immediately after device fabrication, there is little difference in the performance of both solar cells, as detailed in Table 3. This is reasonable since the fraction of aggregated chains in the P3HT films with and without DIO is similar, i.e. at 45 ± 5% (see Table 2). We then moderately annealed the solar cell devices for 18 h at 60 °C (Figure 8b), in order to possibly accelerate C_{60} diffusion into the P3HT layer. After annealing, the performance of the bilayer cell with the P3HT film spun without DIO improved only marginally. In contrast, the cell based on the P3HT film spun with DIO nearly doubled in power conversion efficiency and the fill factor improved from 59% to 67%. Overall, the power conversion efficiencies of these

DOI: 10.1021/acs.macromol.6b01257
Macromolecules 2016, 49, 6420−6430

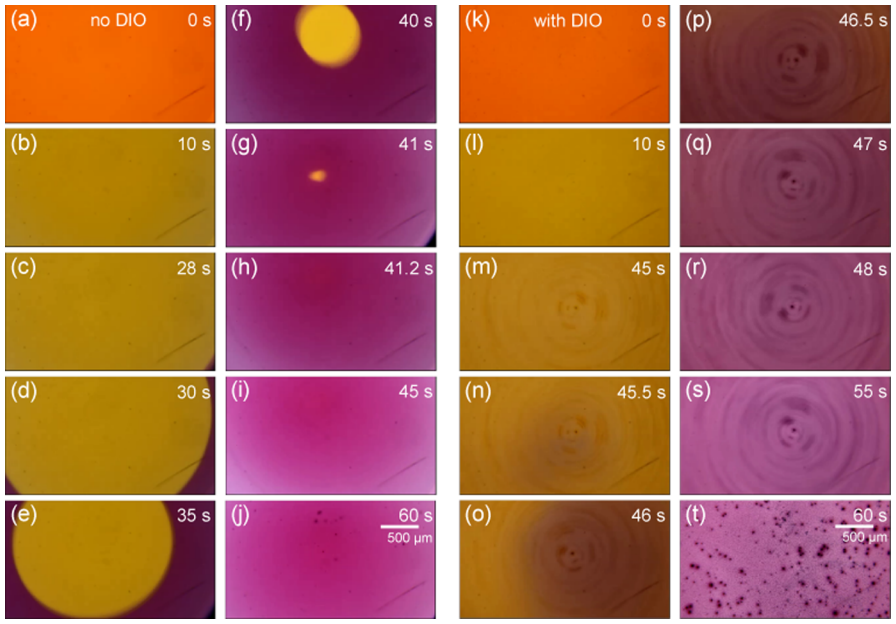

Figure 7. Sequence of optical microscope surface pictures taken in the course of a spin-coating process from a chlorobenzene solution of P3HT (a–j) with and (k–t) without 3 vol % DIO. The quartz substrate is illuminated from below. The spinning times, at which the pictures were taken, are inserted in each picture. The substrate was still at 0 s and at 60 s, and it was rotating in all other picture frames. Orange and yellow areas are liquid and violet areas are solid.

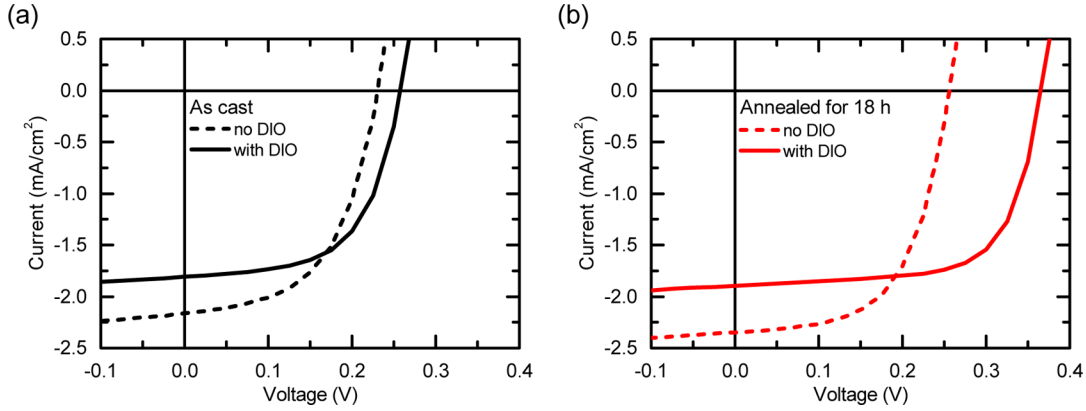

Figure 8. Current–voltage characteristics, at AM1.5 sunlight condition, of organic bilayer solar cells made of C_{60} and P3HT without (dotted lines) and with DIO (solid lines), measured (a) as cast and (b) annealed (60 °C) for 18 h after device fabrication.

Table 3. Fill-Factors (FF) and Power Conversion Efficiencies (PCE) of Organic Bilayer Solar Cells Made of C_{60} and a P3HT Film Spun from a Chlorobenzene Solution without and with 3 vol % DIO, Measured As Cast, after 18 h at 60 °C and after Overall 170 h under AM1.5 Sunlight Condition

	without DIO		with DIO	
P3HT:C60 bilayer solar cell	% FF	% PCE	% FF	% PCE
as cast	53	0.26	59	0.27
annealed for 18 h	58	0.35	67	0.46

bilayer structures are, of course, insufficient, and these devices merely serve as a means to study the influence of the P3HT morphology on the C_{60} diffusion.

We cannot fully exclude that the annealing at 60 °C enhanced the formation of ordered structures in the film spun with DIO, though we note that annealing-driven crystallization usually sets in at temperatures exceeding 100 °C and the similar performance of the cells with films spun without DIO before and after annealing at 60 °C suggests that such an effect seems to be small. We thus consider that the main effect of the moderate annealing is indeed to increase the diffusion coefficient of C_{60}.[53] The enhanced performance of the cell made with the DIO-spun film should thus be attributed to an enhanced amount C_{60} in the P3HT layer. This would not only increase the contact area between P3HT and C_{60}, thus increasing exciton dissociation, but it can also be expected to enhance charge transport to the electrode in a percolative manner.[54] It appears that there is not sufficient free volume (nonaggregated regions) to allow for considerable C_{60}-diffusion, whereas C_{60}-diffusion into a P3HT film prepared with DIO is enabled since the fullerene can diffuse into the larger phases of nonaggregated chains that prevail in the film prepared from a solution with DIO. These observations made on bilayer structures are consistent with the insight gained in blends of P3HT and PCBM that the soluble C_{60} derivative

DOI: 10.1021/acs.macromol.6b01257
Macromolecules 2016, 49, 6420–6430

PCBM diffuses into the nonaggregated areas of P3HT, without affecting the crystal size, structure, or orientation of P3HT.[55−60]

DISCUSSION

The experimental data may be summarized as follows. The kinetics of film formation, shown in Figure 5 and Figure 6, occurs on two distinct time scales, that is (a) the initial formation of a solid film upon spin-coating that occurs within 1 min and (b) the subsequent morphological changes that take place on a time scale of several hours and days, when the film was spun from a solution containing some amount of DIO.

Films spun from CB solution without any DIO in it contain 54% of P3HT in a nonaggregated phase as is evidenced from the absorption spectra, yet the nonaggregated chains are not observed in emission (Figure 3). As already mentioned, this suggests that the phase separation between nonaggregated and aggregated chains is smaller than twice the exciton diffusion length (about 20 nm[19]). In contrast, films spun from CB with DIO in it contain a *larger* amount of nonaggregated phase (60%) after spin-coating than the films spun from only CB. Moreover, the compositional variation between areas richer and poorer in nonaggregated chains is large, with a typical length scale of several μm (Figure 4). The aggregates formed in the film spun from CB with DIO are characterized by a longer conjugation length and concomitantly lower excitonic coupling. When considering the kinetics of film formation, we find that the addition of DIO increases the time t_0 until the aggregate formation sets in from 25 to 39 s, yet it reduces the actual time Δt until the transformation is completed from 20 to 16 s. The process of solidification occurs differently with and without DIO, with a clear advancing solidification front when using only CB, yet an all-over transformation when DIO was added.

It is worth bearing in mind that the surface interactions with the quartz/solvent interface and the solvent/air interface are likely to be dominant driving forces in the solidification process due to the large surface area. This is evidenced, e.g., by the advancing solidification front in the sample without DIO (Figure 7a−j). The addition of DIO does not only alter this surface interaction (Figure 7k−t). It seems that as the CB evaporates (with a boiling point of 132 °C), still dissolved, and thus nonaggregated P3HT chains accumulate in the DIO-richer phase. This is also supported by the in situ absorption measurements. The addition of DIO keeps the P3HT chains in a liquid phase for much longer (about another 15 s, see Figures 6 and 7) even though the CB evaporates, so that eventually a heterogeneous nucleation process seems to occur in place of the surface-induced crystallization.

The boiling point of DIO is 364 °C, and evidently traces of DIO initially remain in the film after spin-coating. We consider that the crystallization in the solid state proceeds as these traces diffuse out of the film on a time scale of hours and days. The process of adding DIO before spin-coating leads to a reduced fraction of aggregates immediately after spin-coating as compared to the films spun without DIO. However, after the crystallization in the solid state finally an equal or even slightly higher fraction of aggregates is obtained with a longer conjugation length.

CONCLUSION

While it is well-known that adding a small amount of the high boiling point solvent DIO to a polymer solution is a means to obtain aggregated chains,[26] the mechanism by which the DIO alters the film formation during spin-coating is not well understood. Our investigations have shown that while the addition of DIO ultimately leads to a similar, only slightly higher amount of aggregated chains in the film, it impacts strongly on the formation mechanism of the film morphology. As a result, the crystalline areas differ in the exciton coupling within the crystallites and morphological distribution between films spun with and without DIO. Our results may point the way to the systematic optimization of films for solar cell or for OFET purposes, even for other semicrystalline polymers.

ASSOCIATED CONTENT

Supporting Information

The Supporting Information is available free of charge on the ACS Publications website at DOI: 10.1021/acs.macromol.6b01257.

Photoluminescence (PL) spectra pertaining to the scale bar of the PL mapping, PL spectra indicating the spectral changes over 48 h, graphics illustrating the spectral deconvolution of the absorption spectra, and time-resolved absorption spectra of P3HT without DIO at 275 K and of P3HT without DIO yet with PCBM at 295 K (PDF)

AUTHOR INFORMATION

Corresponding Author

*(A.K.) E-mail: anna.koehler@uni-bayreuth.de.

Notes

The authors declare no competing financial interest.

ACKNOWLEDGMENTS

We gratefully acknowledge support from the Hanns-Seidel-Stiftung through a stipend to MR by funds from the German Federal Ministry of Education and Research (BMBF), support from the German Science Foundation (DFG) through the Research Training Group GRK 1640 “Photophysics of Synthetic and Biological Multichromophoric Systems“ and from the State of Bavaria through the Research Network “Solar Technologies go Hybrid”. SB and RH acknowledge additional funding from DFG (HI1508/2). RH is also supported by Elite Network Bavaria within the program Macromolecular Sciences. We also thank Tobias Hahn for the help with the solar cell measurements and Markus Hund and Markus Drechsler for the help with the AFM setup and the TEM measurements.

REFERENCES

(1) Ma, W. L.; Yang, C. Y.; Gong, X.; Lee, K.; Heeger, A. J. Thermally stable, efficient polymer solar cells with nanoscale control of the interpenetrating network morphology. *Adv. Funct. Mater.* **2005**, *15*, 1617−1622.

(2) Liu, Y. H.; Zhao, J. B.; Li, Z. K.; Mu, C.; Ma, W.; Hu, H. W.; Jiang, K.; Lin, H. R.; Ade, H.; Yan, H. Aggregation and morphology control enables multiple cases of high-efficiency polymer solar cells. *Nat. Commun.* **2014**, *5*, 5293.

(3) Li, G.; Zhu, R.; Yang, Y. Polymer solar cells. *Nat. Photonics* **2012**, *6*, 153−161.

(4) Liu, X. L.; Hüttner, S.; Rong, Z. X.; Sommer, M.; Friend, R. H. Solvent Additive Control of Morphology and Crystallization in Semiconducting Polymer Blends. *Adv. Mater.* **2012**, *24*, 669−674.

(5) Dang, M. T.; Hirsch, L.; Wantz, G.; Wuest, J. D. Controlling the Morphology and Performance of Bulk Heterojunctions in Solar Cells. Lessons Learned from the Benchmark Poly(3-hexylthiophene):[6,6]-

DOI: 10.1021/acs.macromol.6b01257
Macromolecules 2016, 49, 6420−6430

Phenyl-C-61-butyric Acid Methyl Ester System. *Chem. Rev.* **2013**, *113*, 3734−3765.
(6) Hayer, A.; Khan, A. L. T.; Friend, R. H.; Köhler, A. Morphology dependence of the triplet excited state formation and absorption in polyfluorene. *Phys. Rev. B: Condens. Matter Mater. Phys.* **2005**, *71*, 241302.
(7) Khan, A. L. T.; Sreearunothai, P.; Herz, L. M.; Banach, M. J.; Köhler, A. Morphology-dependent energy transfer within polyfluorene thin films. *Phys. Rev. B: Condens. Matter Mater. Phys.* **2004**, *69*, 085201.
(8) Dou, F.; Buchaca-Domingo, E.; Sakowicz, M.; Rezasoltani, E.; McCarthy-Ward, T.; Heeney, M.; Zhang, X. P.; Stingelin, N.; Silva, C. The effect of phase morphology on the nature of long-lived charges in semiconductor polymer:fullerene systems. *J. Mater. Chem. C* **2015**, *3*, 3722−3729.
(9) Silva, C.; Russell, D. M.; Dhoot, A. S.; Herz, L. M.; Daniel, C.; Greenham, N. C.; Arias, A. C.; Setayesh, S.; Mullen, K.; Friend, R. H. Exciton and polaron dynamics in a step-ladder polymeric semiconductor: the influence of interchain order. *J. Phys.: Condens. Matter* **2002**, *14*, 9803−9824.
(10) Gruber, M.; Wagner, J.; Klein, K.; Hormann, U.; Opitz, A.; Stutzmann, M.; Brütting, W. Thermodynamic Efficiency Limit of Molecular Donor-Acceptor Solar Cells and its Application to Diindenoperylene/C60-Based Planar Heterojunction Devices. *Adv. Energy Mater.* **2012**, *2*, 1100−1108.
(11) Scarongella, M.; De Jonghe-Risse, J.; Buchaca-Domingo, E.; Causa, M.; Fei, Z. P.; Heeney, M.; Moser, J. E.; Stingelin, N.; Banerji, N. A Close Look at Charge Generation in Polymer:Fullerene Blends with Microstructure Control. *J. Am. Chem. Soc.* **2015**, *137*, 2908−2918.
(12) Scarongella, M.; Paraecattil, A. A.; Buchaca-Domingo, E.; Douglas, J. D.; Beaupre, S.; McCarthy-Ward, T.; Heeney, M.; Moser, J. E.; Leclerc, M.; Frechet, J. M. J.; et al. The influence of microstructure on charge separation dynamics in organic bulk heterojunction materials for solar cell applications. *J. Mater. Chem. A* **2014**, *2*, 6218−6230.
(13) Sirringhaus, H.; Brown, P. J.; Friend, R. H.; Nielsen, M. M.; Bechgaard, K.; Langeveld-Voss, B. M. W.; Spiering, A. J. H.; Janssen, R. A. J.; Meijer, E. W.; Herwig, P.; et al. Two-dimensional charge transport in self-organized, high-mobility conjugated polymers. *Nature* **1999**, *401*, 685−688.
(14) Chang, J. F.; Sun, B. Q.; Breiby, D. W.; Nielsen, M. M.; Solling, T. I.; Giles, M.; McCulloch, I.; Sirringhaus, H. Enhanced mobility of poly(3-hexylthiophene) transistors by spin-coating from high-boiling-point solvents. *Chem. Mater.* **2004**, *16*, 4772−4776.
(15) Kline, R. J.; McGehee, M. D.; Kadnikova, E. N.; Liu, J. S.; Frechet, J. M. J. Controlling the field-effect mobility of regioregular polythiophene by changing the molecular weight. *Adv. Mater.* **2003**, *15*, 1519−1522.
(16) Pingel, P.; Zen, A.; Abellon, R. D.; Grozema, F. C.; Siebbeles, L. D. A.; Neher, D. Temperature-Resolved Local and Macroscopic Charge Carrier Transport in Thin P3HT Layers. *Adv. Funct. Mater.* **2010**, *20*, 2286−2295.
(17) Kim, N.-K.; Jang, S.-Y.; Pace, G.; Caironi, M.; Park, W.-T.; Khim, D.; Kim, J.; Kim, D.-Y.; Noh, Y.-Y. High-Performance Organic Field-Effect Transistors with Directionally Aligned Conjugated Polymer Film Deposited from Pre-Aggregated Solution. *Chem. Mater.* **2015**, *27*, 8345−8353.
(18) An, T. K.; Kang, I.; Yun, H. J.; Cha, H.; Hwang, J.; Park, S.; Kim, J.; Kim, Y. J.; Chung, D. S.; Kwon, S. K.; et al. Solvent additive to achieve highly ordered nanostructural semicrystalline DPP copolymers: toward a high charge carrier mobility. *Adv. Mater.* **2013**, *25*, 7003−7009.
(19) Köhler, A.; Bässler, H. *Electronic Processes in Organic Semiconductors: An Introduction*. Wiley-VCH: Weinheim, Germany, 2015.
(20) Despotopoulou, M. M.; Frank, C. W.; Miller, R. D.; Rabolt, J. F. Kinetics of chain organization in ultrathin poly(di-n-hexylsilane) films. *Macromolecules* **1996**, *29*, 5797−5804.
(21) Chen, S. H.; Su, A. C.; Han, S. R.; Chen, S. A.; Lee, Y. Z. Molecular aggregation and luminescence properties of bulk poly(2,5-di-n-octyloxy-1,4-phenylenevinylene). *Macromolecules* **2004**, *37*, 181−186.
(22) Collison, C. J.; Rothberg, L. J.; Treemaneekarn, V.; Li, Y. Conformational effects on the photophysics of conjugated polymers: A two species model for MEH-PPV spectroscopy and dynamics. *Macromolecules* **2001**, *34*, 2346−2352.
(23) Scharsich, C.; Lohwasser, R. H.; Sommer, M.; Asawapirom, U.; Scherf, U.; Thelakkat, M.; Neher, D.; Köhler, A. Control of aggregate formation in poly(3-hexylthiophene) by solvent, molecular weight, and synthetic method. *J. Polym. Sci., Part B: Polym. Phys.* **2012**, *50*, 442−453.
(24) Scharsich, C.; Fischer, F. S. U.; Wilma, K.; Hildner, R.; Ludwigs, S.; Köhler, A. Revealing Structure Formation in PCPDTBT by Optical Spectroscopy. *J. Polym. Sci., Part B: Polym. Phys.* **2015**, *53*, 1416−1430.
(25) Lee, J. K.; Ma, W. L.; Brabec, C. J.; Yuen, J.; Moon, J. S.; Kim, J. Y.; Lee, K.; Bazan, G. C.; Heeger, A. J. Processing additives for improved efficiency from bulk heterojunction solar cells. *J. Am. Chem. Soc.* **2008**, *130*, 3619−3623.
(26) Peet, J.; Brocker, E.; Xu, Y.; Bazan, G. C. Controlled β-Phase Formation in Poly(9,9-di-n-octylfluorene) by Processing with Alkyl Additives. *Adv. Mater.* **2008**, *20*, 1882−1885.
(27) Peet, J.; Kim, J. Y.; Coates, N. E.; Ma, W. L.; Moses, D.; Heeger, A. J.; Bazan, G. C. Efficiency enhancement in low-bandgap polymer solar cells by processing with alkane dithiols. *Nat. Mater.* **2007**, *6*, 497−500.
(28) Clarke, T. M.; Peet, J.; Lungenschmied, C.; Drolet, N.; Lu, X. H.; Ocko, B. M.; Mozer, A. J.; Loi, M. A. The role of emissive charge transfer states in two polymer-fullerene organic photovoltaic blends: tuning charge photogeneration through the use of processing additives. *J. Mater. Chem. A* **2014**, *2*, 12583−12593.
(29) Zhang, F. L.; Jespersen, K. G.; Bjorstrom, C.; Svensson, M.; Andersson, M. R.; Sundstrom, V.; Magnusson, K.; Moons, E.; Yartsev, A.; Inganas, O. Influence of solvent mixing on the morphology and performance of solar cells based on polyfluorene copolymer/fullerene blends. *Adv. Funct. Mater.* **2006**, *16*, 667−674.
(30) Peet, J.; Cho, N. S.; Lee, S. K.; Bazan, G. C. Transition from Solution to the Solid State in Polymer Solar Cells Cast from Mixed Solvents. *Macromolecules* **2008**, *41*, 8655−8659.
(31) Arca, F.; Loch, M.; Lugli, P. Enhancing Efficiency of Organic Bulkheterojunction Solar Cells by Using 1,8-Diiodooctane as Processing Additive. *IEEE J. Photovolt.* **2014**, *4*, 1560−1565.
(32) Yao, Y.; Hou, J. H.; Xu, Z.; Li, G.; Yang, Y. Effect of solvent mixture on the nanoscale phase separation in polymer solar cells. *Adv. Funct. Mater.* **2008**, *18*, 1783−1789.
(33) Buchaca-Domingo, E.; Ferguson, A. J.; Jamieson, F. C.; McCarthy-Ward, T.; Shoaee, S.; Tumbleston, J. R.; Reid, O. G.; Yu, L.; Madec, M. B.; Pfannmoller, M.; et al. Additive-assisted supramolecular manipulation of polymer:fullerene blend phase morphologies and its influence on photophysical processes. *Mater. Horiz.* **2014**, *1*, 270−279.
(34) Venkatesan, S.; Ngo, E. C.; Chen, Q. L.; Dubey, A.; Mohammad, L.; Adhikari, N.; Mitul, A.; Qiao, Q. Q. Benzothiadiazole-based polymer for single and double junction solar cells with high open circuit voltage. *Nanoscale* **2014**, *6*, 7093−7100.
(35) Rogers, J. T.; Schmidt, K.; Toney, M. F.; Bazan, G. C.; Kramer, E. J. Time-Resolved Structural Evolution of Additive-Processed Bulk Heterojunction Solar Cells. *J. Am. Chem. Soc.* **2012**, *134*, 2884−2887.
(36) Park, S.; Nam, S.; Seo, J.; Jeong, J.; Lee, S.; Kim, H.; Kim, Y. Effect of halogen-terminated additives on the performance and the nanostructure of all-polymer solar cells. *J. Korean Phys. Soc.* **2015**, *66*, 521−525.
(37) Kohn, P.; Rong, Z. X.; Scherer, K. H.; Sepe, A.; Sommer, M.; Müller-Buschbaum, P.; Friend, R. H.; Steiner, U.; Hüttner, S. Crystallization-Induced 10-nm Structure Formation in P3HT/PCBM Blends. *Macromolecules* **2013**, *46*, 4002−4013.
(38) Schmidt-Hansberg, B.; Sanyal, M.; Klein, M. F. G.; Pfaff, M.; Schnabel, N.; Jaiser, S.; Vorobiev, A.; Muller, E.; Colsmann, A.; Scharfer, P.; et al. Moving through the Phase Diagram: Morphology

DOI: 10.1021/acs.macromol.6b01257
Macromolecules 2016, 49, 6420−6430

Formation in Solution Cast Polymer-Fullerene Blend Films for Organic Solar Cells. *ACS Nano* **2011**, *5*, 8579−8590.
(39) Kim, Y.; Kim, G.; Lee, J.; Lee, K. Morphology controlled bulk-heterojunction layers of fully electro-spray coated organic solar cells. *Sol. Energy Mater. Sol. Cells* **2012**, *105*, 272−279.
(40) Strobl, G. *The Physics of Polymers*. Springer: Berlin, 1997.
(41) Keller, A.; Cheng, S. Z. D. The role of metastability in polymer phase transitions. *Polymer* **1998**, *39*, 4461−4487.
(42) Reiter, G. Model experiments for a molecular understanding of polymer crystallization. *J. Polym. Sci., Part B: Polym. Phys.* **2003**, *41*, 1869−1877.
(43) Baderschneider, S.; Scherf, U.; Köhler, J.; Hildner, R. Influence of the Conjugation Length on the Optical Spectra of Single Ladder-Type (p-Phenylene) Dimers and Polymers. *J. Phys. Chem. A* **2016**, *120*, 233−240.
(44) Schwarz, C.; Bässler, H.; Bauer, I.; Koenen, J. M.; Preis, E.; Scherf, U.; Köhler, A. Does conjugation help exciton dissociation? A study on poly(p-phenylene)s in planar heterojunctions with C60 or TNF. *Adv. Mater.* **2012**, *24*, 922−925.
(45) Clark, J.; Chang, J. F.; Spano, F. C.; Friend, R. H.; Silva, C. Determining exciton bandwidth and film microstructure in polythiophene films using linear absorption spectroscopy. *Appl. Phys. Lett.* **2009**, *94*, 163306.
(46) Spano, F. C.; Silva, C. H- and J-aggregate behavior in polymeric semiconductors. *Annu. Rev. Phys. Chem.* **2014**, *65*, 477−500.
(47) Spano, F. C. Modeling disorder in polymer aggregates: the optical spectroscopy of regioregular poly(3-hexylthiophene) thin films. *J. Chem. Phys.* **2005**, *122*, 234701.
(48) Gierschner, J.; Huang, Y. S.; Van Averbeke, B.; Cornil, J.; Friend, R. H.; Beljonne, D. Excitonic versus electronic couplings in molecular assemblies: the importance of non-nearest neighbor interactions. *J. Chem. Phys.* **2009**, *130*, 044105.
(49) Panzer, F.; Sommer, M.; Bässler, H.; Thelakkat, M.; Köhler, A. Spectroscopic Signature of Two Distinct H-Aggregate Species in Poly(3-hexylthiophene). *Macromolecules* **2015**, *48*, 1543−1553.
(50) Clark, J.; Silva, C.; Friend, R. H.; Spano, F. C. Role of intermolecular coupling in the photophysics of disordered organic semiconductors: aggregate emission in regioregular polythiophene. *Phys. Rev. Lett.* **2007**, *98*, 206406.
(51) Kuehn, S.; Pingel, P.; Breusing, M.; Fischer, T.; Stumpe, J.; Neher, D.; Elsaesser, T. High-Resolution Near-Field Optical Investigation of Crystalline Domains in Oligomeric PQT-12 Thin Films. *Adv. Funct. Mater.* **2011**, *21*, 860−868.
(52) Chang, L. L.; Lademann, H. W. A.; Bonekamp, J. B.; Meerholz, K.; Moule, A. J. Effect of Trace Solvent on the Morphology of P3HT:PCBM Bulk Heterojunction Solar Cells. *Adv. Funct. Mater.* **2011**, *21*, 1779−1787.
(53) Fischer, F.; Hahn, T.; Bässler, H.; Bauer, I.; Strohriegl, P.; Köhler, A. Measuring Reduced C-60 Diffusion in Crosslinked Polymer Films by Optical Spectroscopy. *Adv. Funct. Mater.* **2014**, *24*, 6172−6177.
(54) Yin, W.; Dadmun, M. A New Model for the Morphology of P3HT/PCBM Organic Photovoltaics from Small-Angle Neutron Scattering: Rivers and Streams. *ACS Nano* **2011**, *5*, 4756−4768.
(55) Treat, N. D.; Brady, M. A.; Smith, G.; Toney, M. F.; Kramer, E. J.; Hawker, C. J.; Chabinyc, M. L. Interdiffusion of PCBM and P3HT Reveals Miscibility in a Photovoltaically Active Blend. *Adv. Energy Mater.* **2011**, *1*, 82−89.
(56) Chen, D.; Liu, F.; Wang, C.; Nakahara, A.; Russell, T. P. Bulk heterojunction photovoltaic active layers via bilayer interdiffusion. *Nano Lett.* **2011**, *11*, 2071−2078.
(57) Kiel, J. W.; Eberle, A. P.; Mackay, M. E. Nanoparticle agglomeration in polymer-based solar cells. *Phys. Rev. Lett.* **2010**, *105*, 168701.
(58) Campoy-Quiles, M.; Ferenczi, T.; Agostinelli, T.; Etchegoin, P. G.; Kim, Y.; Anthopoulos, T. D.; Stavrinou, P. N.; Bradley, D. D.; Nelson, J. Morphology evolution via self-organization and lateral and vertical diffusion in polymer:fullerene solar cell blends. *Nat. Mater.* **2008**, *7*, 158−164.
(59) Pfannmöller, M.; Flügge, H.; Benner, G.; Wacker, I.; Sommer, C.; Hanselmann, M.; Schmale, S.; Schmidt, H.; Hamprecht, F. A.; Rabe, T.; et al. Visualizing a homogeneous blend in bulk heterojunction polymer solar cells by analytical electron microscopy. *Nano Lett.* **2011**, *11*, 3099−3107.
(60) Kozub, D. R.; Vakhshouri, K.; Orme, L. M.; Wang, C.; Hexemer, A.; Gomez, E. D. Polymer Crystallization of Partially Miscible Polythiophene/Fullerene Mixtures Controls Morphology. *Macromolecules* **2011**, *44*, 5722−5726.

DOI: 10.1021/acs.macromol.6b01257
Macromolecules 2016, 49, 6420−6430